Hittite Journal of Science and Engineering, 2015, 2 (1) 65-76
ISSN NUMBER: 2149-2123
DOI: 10.17350/HJSE19030000010

Hillock Formation by Surface Drift-Diffusion Driven by the Gradient of Elastic Dipole Interaction Energy Under Compressive Stresses in Bi-Crystalline Thin Films

Tarik Omer Ogurtani[1] and Oncu Akyildiz[2]
[1] Middle East Technical University, Department of Metallurgical and Materials Engineering, Ankara, TURKEY.
[2] Hitit University, Department of Metallurgical and Materials Engineering, Corum, TURKEY.

ABSTRACT

We investigated surface drift diffusion induced grain boundary (GB) grooving and ridge (hillock) formation and growth, under the combined actions of the capillary forces and applied uniaxial compressive stresses, in bi-crystal thin films with dynamical computer simulations. In the present theory, the generalized driving force for the stress induced surface drift diffusion includes not only the usual gradient of the elastic strain energy density, but also the elastic dipole tensor interaction energy. During the morphological evolution of GB ridge formation and growth, triple junction (TJ) displacement and its velocity are continuously tracked down in order to resolve precisely the crossover time and depth at which velocity sign inversion takes place. An incubation time for the onset of the ridge growth stage coupled to the GB-TJ displacement velocity inversion is defined and its dependence on the stress is investigated. This analysis implies that the ridge growth stage is not controlled by Ziegler's 'maximum entropy production principle' but rather Prigogine's 'minimum entropy production hypothesis' for the stationary non-equilibrium states in complex systems, which are exposed to external applied body forces and surface tractions.

Key Words:
Grain Boundary Grooving; Non-Equilibrium Thermodynamics; Surface/Grain Boundary Diffusion; Compressive Stresses; Thin Films.

Article History:
Received: 2015/05/07
Accepted: 2014/06/15
Online: 2015/07/01

***Correspondence to**: Tarık Omer Ogurtanı, Middle East Technical University, Faculty of Engineering, Department of Metallurgical and Materials Engineering, Ankara, Turkey*
Tel: +90 (312) 210-2512
Fax: +90 (312) 210-1267
E-Mail: ogurtani@metu.edu.tr

INTRODUCTION

Abbreviations:

GB	: grain boundary;
TJ	: triple junction;
EDTI	: elastic dipole tensor interaction;
ESED	: elastic strain energy density

Grain boundary (GB) thermal grooving is a capillary driven surface morphological evolution, and observed in the vicinity of the grain boundary- free surface junctions in polycrystalline materials at rather elevated temperatures. When the underlying bulk system is exposed to the external and/or internal stress fields the problem becomes much more complicated. One of the most widely employed method to study the effects force fields on the GB grooving, is to couple the capillary-driven surface diffusion with the steady state atomic flux induced by the normal component of the surface traction acting on the GB layer.

Following this approach Genin et al. [1] extended Mullins' [2] classical theory of thermal grooving to study the development of an isolated groove with constant GB flux due to normal compressive stress gradients (i.e., Herrings' force) acting on the GB layer. They observed stagnation of the groove formation under compressive stresses.

In addition to GB grooving, the formation and development of ridges or hillocks is one of the most commonly observed surface reconstruction phenomena in polycrystalline thin films. *In situ* observations of thin films revealed that ridges generally form in the vicinity of GB TJs; and it is thought that they form under the influence of residual and/or thermo-mechanical compressive stresses, induced during the deposition

and/or the thermal cycling processes, respectively [3–9].

One of the drawbacks of the study of Genin and coworkers [1, 6, 7] was the absence of long range surface diffusion into the ridge from the surroundings film area. Kim et al. [9] indicated the essence of long range diffusion by citing Chaudhari's [10] ridge model in which an analysis of the lattice diffusion (Nabarro – Herring creep) was presented. Presland et al. [11], on the other hand, provided the evidence for the surface diffusion controlled mechanism during ridge growth in silver thin films. These authors directly adopt the results of the Hull-Rimmer theory [12] by noting the similarity between the two problems, ridge growth and GB void growth, after making suitable arrangements. As a result, they obtained a ridge growth rate which is linearly proportional with the applied stresses. Gao et al. [13] and Zhang and Gao [14] have studied constrained grain boundary diffusion coupled with the surface diffusion, leading to formation of crack-type wedges via mass transfer between grain boundary region and the free surface of the film. The proposed coupling relies on the crack tip curvature and its higher derivatives (See: Eqs. 13 and 14 of reference 14) where, the surface drift diffusion considered in their treatment is of Mullins type, which is completely controlled by the capillary forces acting along the free surfaces and there was no attempt to consider the gradient of hydrostatic part of stress tensor as a driving force.

The elastic strain energy density (ESED) gradient driven instability is predicted to occur for stresses of either sign (quadratic stress dependence). However, for a kinetically driven instability, if the interface is unstable for a given stress state, then it should necessarily be stable for the opposite stress state or vice versa [15]. Lahiri [16] studied ridges on a Pb thin film and observed the effect of stress sign reversal: The ridges grow under compressive stresses and shrink in height under tensile stresses. Similarly, Barvosa-Carter et al. [15] demonstrated that the corrugated Si (001) interface is stable under tensile and roughens under compressive stresses. It is evident that ESED cannot play any role in the sign reversal behavior observed in surface morphological evolutions but a term with a linear stress dependence can.

In this paper, we considered the role of the gradient of the hydrostatic part the stress tensor generated by the applied uniaxial compressive stress system as a driving force on the surface drift diffusion (via isotropic surface point defects) through the elastic dipole tensor interaction (EDTI), which was proposed and elaborated by Ogurtani [22] and presented briefly in Appendix. The EDTI is accounted for the interactions in the bulk phases between the strain field of the mobile atomic carriers (mono-vacancies or paraelastic defects such as Frenkel defects) and the local stress fields. EDTI is also valid for the mobile defects 'ad atoms' lying at the surface layer as well as in the grain boundary region as demonstrated by Kirchheim [18] in his well-accepted classical work. Later, other authors also employed the concept for bulk [19] and grain boundary [20] diffusion. According to our best knowledge, excluding our recent work on the effects of applied uniaxial tension stresses on GB grooving [21], there exists neither gross scale simulation nor analytical work that reflects the dominant effect of long range surface drift-diffusion driven by the stress gradient in the literature. The main reason for this is that the surface is always assumed to be traction free, and thus the Herring's force vanishes identically (see Appendix).

The present computer simulation experiments emphasize the crucial role played by the EDTI as driving force for surface diffusion in explaining the GB grooving under compressive stresses as well as the ridge formation at the GBs. In these experiments, we did not take into account the particle flux coming from or going through the GB region (evaluated at the TJ) directly. In other words, we assumed that the material drainage at the GB-groove tip and transfer through the GB by the non-vanishing stress field gradients as well as by the concentration inhomogeneities of the mobile species is negligibly small compared to the material excavation and transport by the stress driven surface drift-diffusion operating along the groove surfaces via EDTI.

Physical and Mathematical Modeling

The thermodynamic composite system under consideration consists of two bulk regions, and a vapor phase. The bulk regions are connected by a GB, and the vapor phase is separated from the solid phase by a singly connected curved surface layer as illustrated in Figure 1. The surface layer and the GB region are both presumed to have finite and invariant thicknesses, denoted as h_s and h_g, respectively.

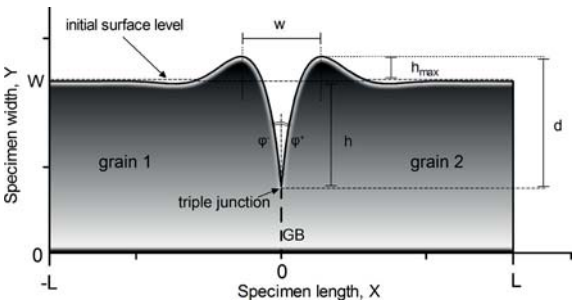

Figure 1. Sketch of a grain boundary groove, which evolves on the upper triple junction, illustrating its width (w), depth (h and d), maxima (hmax) and dihedral angle (φ). Here W and L denote the half film width and length, respectively. The grain boundary extends along the origin. .

a. The governing equation for the surface drift-diffusion and growth

According to the micro-discrete formulation of the irreversible thermodynamics of surfaces and interfaces [22, 23], the evolution kinetics of traction free surfaces exposed to the elastostatic fields in addition to the capillary forces, may be described in terms of surface normal displacement velocities $\bar{V}_{ord}$ by the following well-posed moving boundary value problem in 2D space for ordinary points. In the following expression, normalized and scaled parameters and variables are used, and they are indicated by the bar signs over the letters:

$$\bar{V}_{ord} = \frac{\partial^2}{\partial \bar{\ell}^2}\left(\Delta\bar{g}^o_{vb} + \bar{\kappa} + \Xi\bar{\sigma}_h + \Sigma\bar{\sigma}_h^2\right) - \bar{\mathrm{M}}_{vb}\left(\Delta\bar{g}^o_{vb} + \Sigma\bar{\sigma}_h^2 + \bar{\kappa}\right) \tag{1}$$

In the above expression, $\bar{\ell} \equiv \ell / \ell_o$ is the normalized curvilinear coordinate along the surface (arc length) in 2D space. Here, ℓ_o is the arbitrary length scale, and is chosen as $\ell_o = h_o / 2 \Rightarrow 100$ nm for the present simulation studies, Here, h_o is the thickness of the thin film having a length designated by L_o, which is taken as equal to $L_o = 30\ell_o \Rightarrow 3.0$ μm. This choice implies that the aspect ratio of the test module, denoted by $\beta \equiv L_o / h_o$, is 15. $\Delta\bar{g}^o_{vb}$ denotes the normalized thermal part of the volumetric Gibbs free energy density difference $\breve{g}_{vb} = (\breve{g}^o_v - \breve{g}^o_b)$ between the realistic void phase (vacuum/vapor) and the bulk matrix ($\Delta\bar{g}^o_{vb}$<0 evaporation or void growth). This normalization is done with respect to the specific surface Gibbs free energy of the surface phase denoted by g_s, and it is given by $\Delta\bar{g}_{vb} = \breve{g}_{vb}\ell_o / g_s$, which also involves the length scale or the metric ℓ_o. Similarly, the second group of terms in Eq. (1) is related to the surface growth process, which will not be employed in the present simulation studies ($\Delta\bar{g}^o_{vb} = 0;\ \bar{\mathrm{M}}_{vb} = 0$) to avoid further complications in data interpretations.

In Eq. (1), $\bar{\kappa} = \kappa\ell_o$ is the local curvature and is taken to be positive for a concave solid surface (troughs). Similarly, the positive direction of the surface displacement is assumed to be towards the bulk (matrix) phase, which implies the growth of surface troughs or grooves, and the simultaneous shrinkage of crest regions.

The normalized hoop stress is denoted by, $\bar{\sigma}_h = \sigma_h / \sigma^o_h$, which was normalized with respect to the nominal stress applied at the edges of the specimen, σ_o. The hoop stress in plane strain condition may be defined by $\sigma_h = \hat{t}.\underline{\underline{\sigma}}.\hat{t}$, where $\hat{t}$ is the unit surface tangent vector, and $\underline{\underline{\sigma}}$ is 2D-stress tensor evaluated at the bulk region just adjacent to the surface layer. The hoop stress for the traction free surfaces may be given by the following exact connection: $\sigma_h = Tr\underline{\underline{\sigma}}$ since $\hat{n}.\underline{\underline{\sigma}}.\hat{n} = 0$ for traction free surfaces. The double under bars indicate tensor quantities. Ξ designates the elastic dipole tensor interaction (EDTI) parameter, which is given by the expression $\Xi = (1+\nu)\ell_o\sigma^o_h\, Tr\underline{\underline{\lambda}} / 3g_s$. Here, $Tr\underline{\underline{\lambda}}$ is the trace of the elastic dipole tensor. For further applications of EDTI on the stress dependent surface growth mobility, one may refer to Ogurtani and Akyildiz [24], Ogurtani and Oren [23]. Similarly, the dimensionless parameter Σ corresponds to the relative value (referred to the capillarity) of the intensity of the elastic strain energy density (ESED) contribution on the stress-driven surface drift-diffusion. For plain strain condition, ESED takes the following form: $\left(\underline{\underline{\sigma}} : \underline{\underline{\varepsilon}} / 2 \rightarrow (1-\nu^2)\sigma_h^2 / 2E\right)$. Here $\underline{\underline{\varepsilon}}$ is the strain tensor, E is the Young's modulus, and ν is the Poisson' ratio. Then one writes $\Sigma = (1-\nu^2)\ell_o\left(\sigma^o_h\right)^2 / 2Eg_s$.

The time and space variables $\{t, \ell\}$ are scaled in the following fashion: first of all, $\hat{\mathrm{M}}_s = (D_s h_s / \Omega_s kT)$, an atomic mobility associated with the mass flow at the surface layer is defined and then a new time scale is introduced by $\tau_o = \ell_o^4 / \left(\Omega_s^2 \hat{\mathrm{M}}_s g_s\right)$. Here, Ω_s and D_s are the mean atomic volume of chemical species in the surface layer and the isotropic part (*i.e.*, the minimum value) of the surface diffusion coefficient respectively. The generalized mobility, $\hat{\mathrm{M}}_{vb}$, associated with interfacial displacement reaction taking place during the surface growth process (adsorption or desorption) is also normalized with respect to the mobility of the surface diffusion, $\hat{\mathrm{M}}_s$, and is given by $\bar{\mathrm{M}}_{vb} = \hat{\mathrm{M}}_{vb}\ell_o^2 / \hat{\mathrm{M}}_s$. The normalized time $\bar{t}$ and the test module thickness $\bar{h}_o$ used in the present simulations are defined by $\bar{t} = t / \tau_o$, and $\bar{h}_o = h_o / \ell_o$, respectively.

TJ drift velocity along the rigid GB can be represented by [22, 23]:

$$\bar{V}^{long}_g = \bar{\mathrm{M}}^{long}\frac{\Omega_g d_a}{2\Omega_s^2 h_g}\left[2\lambda - \left(\cos\varphi^+ + \cos\varphi^-\right)\right] \tag{2}$$

Here, d_a, and Ω_g are the interatomic distance and mean atomic volumes of chemical species in the GB layer, respectively. $\bar{M}^{long}$ is the longitudinal generalized mobility of the TJ, which is defined below. φ^+ and φ^- are the dihedral angles as illustrated in Figure 1. λ is the wetting parameter associated with the TJ, which is assumed to be isotropic in the present case study. It may be given by $\lambda = g_g / 2g_s$, where g_g is the specific surface Gibbs free energy associated with the GB.

The following boundary conditions at the TJ in terms of right and left side fluxes associated with the surface layer may be written;

$$\bar{J}^{\mp}_o = \mp\bar{\mathrm{M}}^{long}\frac{\bar{d}_a}{2\bar{\Omega}_s^2}\left(\lambda - \cos\varphi^{\mp}\right) \mp \bar{J}_g / 2 + \bar{\mathrm{M}}^{trans}\frac{\bar{d}_a}{\bar{\Omega}_s^2}\left(\sin\varphi^+ - \sin\varphi^-\right) \tag{3}$$

In the above equation, the ($\mp$) first group of terms

represents the material lost from the TJ-edge of the GB layer due to shortening of its length caused by the GB-TJ longitudinal motion, and then injected equally into the both branches of the surface layer to extend its length (*in situ* 2D-phase transition). The last group of terms corresponds to the mass transfer from one side of the surface layer to another side through the GB-TJ region to compensate the asymmetry in the surface groove profile till the non-equilibrium stationary state having symmetrically disposed configuration is attained asymptotically. Here, the particular partition of the incoming GB flux $\overline{J}_g$ between $\overline{J}_o^+$ and $\overline{J}_o^-$ at the GB-TJ is a matter of convenience; otherwise it is completely arbitrary as long as one satisfies the generalized law of conservation of particles including the *in situ* phase transformation at the TJ. Here, the positive direction of the surface flux $\overline{J}_o^{\mp}$ is taken along the clock-wise direction enclosing sidewalls of the finite specimen in 2D space. Similarly, $\overline{J}_g$ denotes the normalized atomic flux associated with the incoming GB mass flow evaluated just at the GB-TJ. In the present simulation studies, the atomic grain boundary flux term $\overline{J}_g$ is not considered.

$\overline{\mathrm{M}}^{trans}$ corresponds to the normalized transverse mobility of the TJ with respect to $\hat{\mathrm{M}}_s$. The explicit expressions may be given by:

$$\hat{\mathrm{M}}^{long}=\frac{\mathfrak{R}^{long}}{kT}\frac{h_g}{\Omega_g}\,,\ \hat{\mathrm{M}}^{trans}=\frac{\mathfrak{R}^{trans}}{kT}\frac{h_s}{\Omega_s}\,,\ \hat{\mathrm{M}}_s=\frac{D_s}{kT}\frac{h_s}{\Omega_s} \qquad (4)$$

Where, $\mathfrak{R}^{long}$ and $\mathfrak{R}^{trans}$ are the transition rates associated with the longitudinal and transverse displacements of the TJ, which may be calculated by Eyring [26] transition rate theory.

b. Numerical methods

In the evaluation of the hoop stresses at the top and bottom free surfaces of the thin metallic bicrystal film including GB groove faces we utilize the simplest implementation of the indirect boundary element method (IBEM) [27] which utilizes the mid-positions of the straight line elements in two dimensional space as collocation points. This guarantees the surface smoothness conditions for the validity of the governing Fredholm integral equation of the second kind at the corners and edges. Neumann boundary conditions are employed along the top and bottom surfaces (i.e., surface tractions are zero, $\underline{\underline{\sigma}}.\hat{n}=0$) and prescribed surface normal tractions (i.e., uniaxial compression defined as $\mp\sigma_{xx}\big|_{\pm L}\,\hat{x}$ at $\pm L$) at the specimen edges. The explicit Euler's method combined with the adaptive time step auto-control mechanism is employed in connection with Gear's stiff stable second-order time integration scheme [28] with the initial time step selected in the range of $\left(10^{-8}-10^{-9}\right)$ in the normalized time domain. This so-called adaptive time step procedure combined with the self-recovery effect of the capillary terms guarantees the long-time numerical stability and accuracy of the explicit algorithm even after performing $2^{75}-2^{90}\approx 10^{27}$ steps. An adaptive mesh refining procedure is continuously applied using the criteria advocated by Pan and Cocks [29]. Typically, the number of active collocations points in our discretization scheme varied from 400 to about 550 depending on the normalized applied stress and TJ-longitudinal mobility. The curvature and the normal line vector are evaluated at each node for each time step by using discrete geometric relationships in connection with the fundamental definitions of the radius of curvature in differential geometry.

In our calculations, a few percent unavoidable mass leakage is observed at low stress levels $\left(\Xi\le -0.1\right)$ to the system, which shows appreciable improvements at the moderate to high stress levels $\left(\Xi\ge 1\right)$. This leakage arises from both edges of the test modulus even though we are employing insulating boundary conditions:

$$J_{Edges}=\frac{\partial}{\partial\overline{\ell}}\left(\overline{\kappa}+\Xi\overline{\sigma}_h+\Sigma\overline{\sigma}_h^2\right)\Big|_{L_{\pm}}\to 0$$

The main reason is associated with the fact that one doesn't have enough number of collocation points at the critical spots of the test modulus such as edges and corners, where the extreme high stress concentrations take place. We have also used a special program to compensate this mass leakage at the edges, which adds to or subtracts material from the upper and lower surfaces, respectively, using a well-defined scaling factors. On the other hand, the genuine mass accumulations at the ridges mainly come from the upper and lower surfaces of the specimen, which results as the thinning of the film. This thinning is very hardly noticeable since the sample has a very high length to thickness aspect ratio.

In the next section, while discussing on the simulation results we would often encounter with the time constant and thus it is beneficial to get some idea on the magnitude of the tentative time constant based on the available experimental data in the literature. According to the definitions of the time constant τ_o and the surface mobility $\hat{M}_s$ introduced previously, one may write $\tau_o\equiv\left[kT\ell_o^4/(\Omega_s D_s h_s g_s^o)\right]$, which may be easily calculated using the published physico-chemical data available in the literature. Using the values tabulated for copper in Table 1, one finds that $\tau_o\cong 5.72\times\left[10^{+2}-10^{+6}\right]$ s depending upon the selected scale length ℓ_o $[100\ nm-1000\ nm]$ at $T=573^oK$, which is the standard device accelerated test temperature. At room temperature, $T=300^oK$, one obtains about eight orders of magnitudes higher values for the normalized time such as $\tau_o\cong 1.2\times\left[10^{10}-10^{14}\right]$ s.

Table 1. Physicochemical properties of Al, Cu, Sn, and Pb [38].

	Al	Cu	Sn	Pb
Elastic Moduli (GPa)	70.6	129.8	49.9	16.1
Poisson' Ratio	0.345	0.343	0.35	0.44
Surface tension (nm^{-1})	0.915	1.780	0.685	0.480
$\|tr(\underline{\lambda})\|$	0.69	0.3	0.6	0.6
$Q_s(eV)$	0.62	0.95	0.506	-
$D_s^o(m^2s^{-1})$	$3x10^{-6}$	$5.84x10^{-5}$	$4.9x10^{-4}$	-
$h_s(m)$	$2.86x10^{-10}$	$2.56x10^{-10}$	$5x10^{-10}$	-
$\Omega_s(m^3)$	$1.66x10^{-29}$	$1.18x10^{-29}$	$2.71x10^{-29}$	$3.02x10^{-29}$

RESULTS AND DISCUSSIONS

In this section, first we will compare general features of the profiles obtained under the low uniaxial compressive stress field and the one deduced from the thermal grooving experiment presented in Figure 2d, where only the capillary forces are in action. Then the topological effects of the increase in the applied uniaxial compressive stress are examined critically by altering EDTI parameter covering a wide range of values: [Ξ = −0.1, … ,1,.. −10].

In the present simulations ESED contribution is ignored due to the fact that the EDTI term is at least a few orders of magnitude larger; especially for the medium and low stress levels. Using the values tabulated in Table 1; for a copper film having a thickness of h_o =200 nm with a scaling length ℓ_o =100 nm, the given EDTI interval corresponds to [σ_{Cu}=13.25–1325] MPa, and for aluminum: [σ_{Al}=2.96–296] MPa. These stress ranges yield for ESED, respectively: [$\Sigma_{Cu}=3.5x10^{-5}$,…, $3.5x10^{-1}$] and [$\Sigma_{Al}=6.3x10^{-6}$,…, $6.3x10^{-2}$]. However, as we mentioned previously, the difference between these two parameters decreases as the stress level increase. This is due to the quadratic dependence of ESED rather than the linear dependence of EDTI to the stress. It was found by Ogurtani [22] that the threshold level of the stress was about 21 GPa for the silicon and 15.6 GPa for copper thin crystal films, and above which the elastic strain energy w_{ESED} starts to dominate the elastic dipole tensor interaction energy denoted by u_{EDTI}, according to the relationship: $\{u_{EDTI}/w_{ESED}=-2ETr\underline{\underline{\lambda}}\sigma_o^{-1}/3\}$. The upper stress level employed for the present simulations for 200 nm thick samples can be comparable with findings of Friesen et al. [30] namely, the instantaneous stress level at the initiation of the Volmer–Weber growth of polycrystalline Cu films was lower in the pre-coalescence regime (of order 1 GPa), and increased monotonically up to the film continuity, and then remained constant thereon (of order 10 GPa). Still the 100 nm Cu film deposited on the backside of each cantilever to improve the laser reflectivity did not show any plastic deformation, and showed rather reversible stress evolution during the growth.

Here, the initial configurations of the reported test modulus are always a flat surface having a freshly formed GB cutting the crystal into two pieces. Accordingly; the groove tip displacement is measured with respect to the original surface and the positive direction is chosen towards the bulk phase (Figure 1). In this paper, only the upper half of the test modulus is illustrated, which has reflection symmetry with respect to the mid-plane of the bicrystal.

Successive profiles, given in Figure 2a-b, show that the evolution under a uniaxial compressive stress (Ξ=−0.1) is tend to form a ridge (hillock) at the GB. The groove depth 'h', which is measured from the initial flat surface towards the bulk region, is presented in Figure 2e on a semi log scale with respect to the normalized time. A close inspection shows that the depth follows up a $t^{1/4}$ trajectory after an initial transient stage, which can be categorized as Mullins' type, up to a certain depth where one observes a very pronounce peaking on the plot. This peaking depth may be called as the crossover depth designated by '$\overline{h}_c$', and similarly the corresponding normalized time may be designated as the crossover time for a good reason, and denoted by '$\overline{t}_c$'. If one zooms into the termination region of Figure 2c, it is observed that the GB-TJ displacement velocity is crossing the zero line and changes its sign, and then continues upwards to take negative values but ever decreasing in magnitude, and finally approaches zero line, asymptotically. This peculiar behavior is more pronounced in Figure 3b-4b, where a few orders of magnitude much higher stress is employed. Thus, the crossover time $\overline{t}_c$, where the depth, velocity and hoop stress versus log(time) plots, all show extremal behavior may be designated as the signature for the incubation time for the ridge formation and growth process.

Another characteristic length that was adopted by Mullins for his classical analytical theory; is the depth measured from the position of the peak maxima to the GB-root ($d=h+h_{max}$), and designated by 'd'. It is also illustrated in Figure 3b in log-log scale together with the similar plot for the peak maxima $h_{\max}$. The simulation results presented in Figure 3 are obtained for a factor of ten increase in the

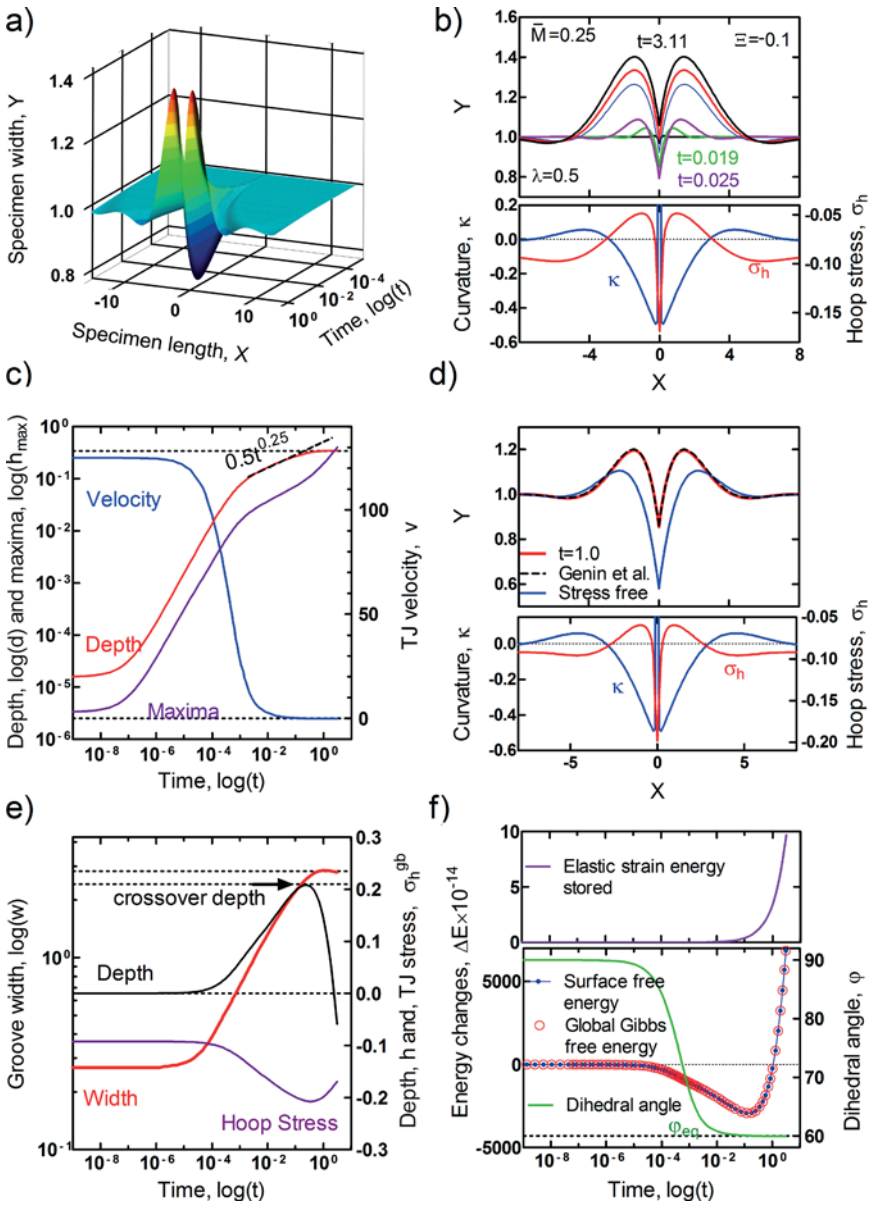

Figure 2. (Color online) Isotropic grain boundary grooving for λ=0.5, $\bar{M}^{long} = \bar{M}^{trans} = \bar{M} = 0.25$ and Ξ=−0.1. a) 3D representation of the groove evolution, b) successive 2D profiles; curvature and hoop stress distributions corresponding to t=3.11 (black profile), c) kinetic data for groove depth ('d'), maxima and TJ velocity, d) comparison of the stress free and groove under tension profiles given by Genin et al. [1] at t=1.0; curvature and hoop stress distributions at t=1.0, e) kinetic data for groove depth ('h'), width and TJ stress, f) energy changes and the kinetic data for the dihedral angle in semi-log scale.

applied nominal stress $\bar{\Xi}$ =1.0, compared to the previous simulation experiment. Figure 3b clearly indicates that the distance from the groove root to the maxima '*d*' shows a well-defined plateau during the ridge growth, even though the peak maxima doesn't show any sign of stagnation but rather elevation. Here a slight overshooting also takes place before the dihedral angle reaches to the non-equilibrium stationary value (Figure 3d-4d). All these indicate that the ridge translates into a nonequilibrium stationary state (according to the definition of Prigogine [31], when the Mullins' depth and width parameters enter into the well-defined plateau regime as may be also seen in Figure 2c-d by zooming if one filters out the white noise associated with the local internal entropy production.

In Figure 3c-4c the kinetics of the groove width and

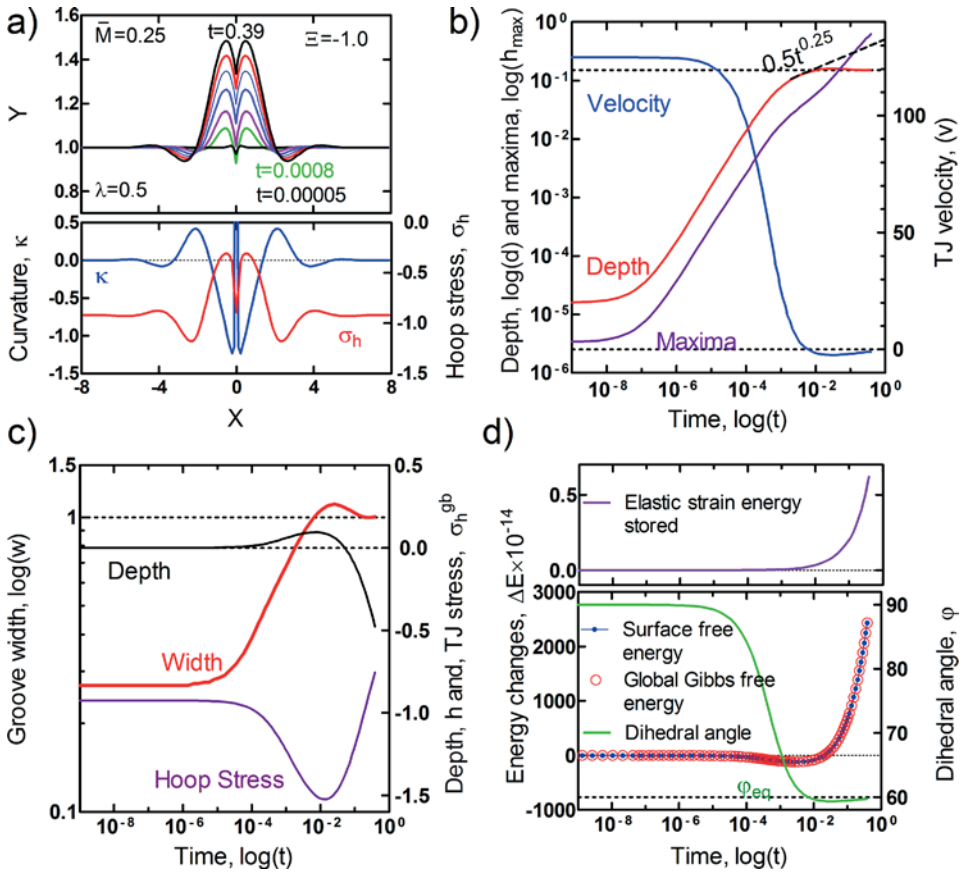

Figure 3. (Color online) Isotropic grain boundary grooving for λ=0.5, $\bar{M}^{long} = \bar{M}^{trans} = \bar{M} = 0.25$ and Ξ=–1.0. a) successive 2D profiles; curvature and hoop stress distributions corresponding to t=0.39 (black profile), b) kinetic data for groove depth ('d'), maxima and TJ velocity, c) kinetic data for groove width, depth ('h') and TJ stress, d) energy changes and the kinetic data for the dihedral angle in semi-log scale.

the value of the hoop stress at the TJ are also demonstrated. The compressive hoop stress value reported in these plots increase in magnitude as the groove deepens to h_c and then decreases as the grain boundary length increases with the ridge formation. On the contrary to the local hoop stress, the groove width stays constant during the plateau region. These are all strong indications for the existence of the ridge as a non-equilibrium stationary state under the given applied constant compressive stress system (isothermal isobaric natural process).

The solution proposed by Genin et al. [1] have also been presented in Figure 2d by reproducing it (using equations 23-27 of aforementioned article) for an arbitrary constant grain boundary flux of j=0.4, and for λ=0.5, B=1.0, and t=1.0. Although there are some fundamental differences, there exists a qualitative agreement between the Genin's analytic solution and the simulated profile in Figure 2. This is due to the fact that the dihedral angle and the GB-TJ velocity reported in Figure 2c-f follow trajectories very similar to the equilibrium trajectories employed in Mullins theory, during the natural evolution of the grain boundary groove at this moderately low stress levels. In the present case, the applied stress directly acts on the surface drift diffusion through the EDTI, while the GB region assumed to play no active role (no gradient driven matter flux is coming out from the GB to the TJ or vice versa, $J_g = 0$) in the overall process. The GB region has only one active role that is the direct involvement in the 2D-phase transition (in situ material exchange) taking place at the GB-TJ during its longitudinal displacement.

The free energy changes presented here in several plots are formulated recently [32] in great details for the isobaric composite system. Such a system is enclosed by external flexible and diathermal boundaries that allow not only establishing thermal equilibrium in the system, but also permitting to have a direct contact with the external constant surface tractions and body forces. That means the work done on the system is non-vanishing, $\Delta W \neq 0$. For such a system having a discrete free surface contour line, letting n to designate the total number of nodes, one may write down the rate of total strain energy relaxation (dissipation power) at a given time step i during the evolution

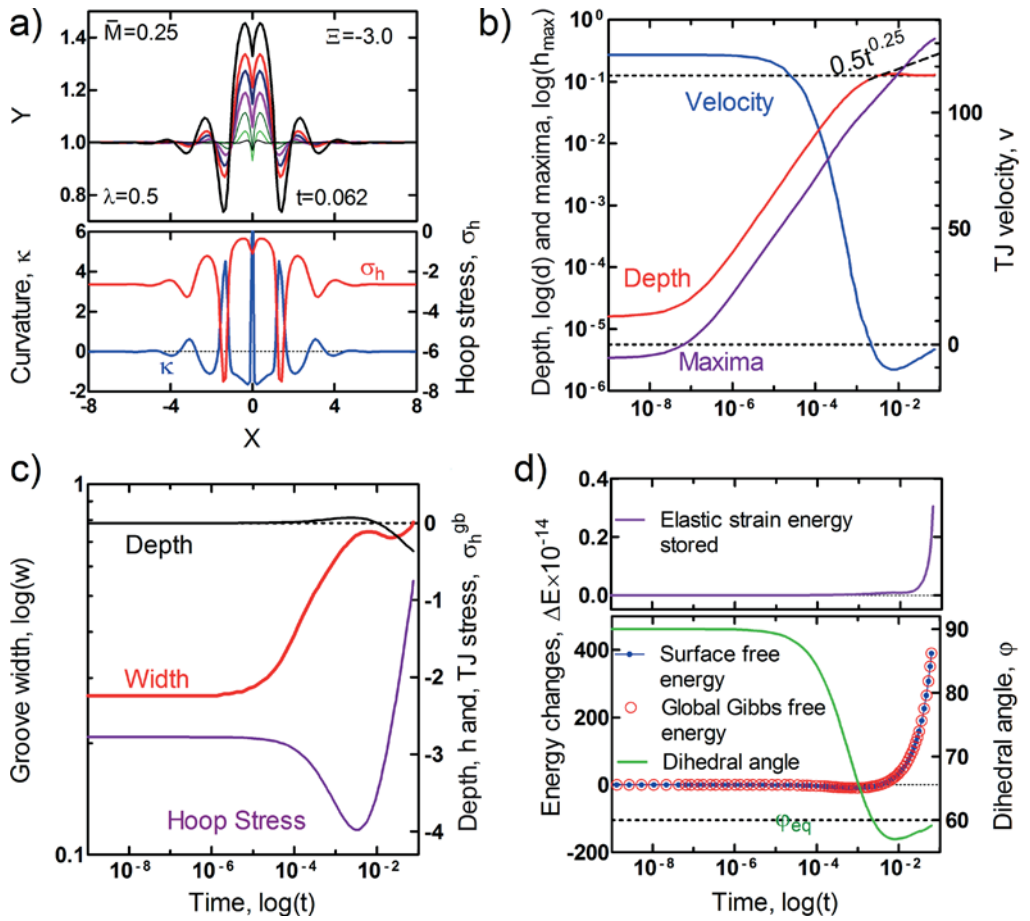

Figure 4. (Color online) Isotropic grain boundary grooving for λ=0.5, $\bar{M}^{long} = \bar{M}^{trans} = \bar{M} = 0.25$ and Ξ=−3.0. a) successive 2D profiles; curvature and hoop stress distributions corresponding to t=0.062 (black profile), b) kinetic data for groove depth ('d'), maxima and TJ velocity, c) kinetic data for groove width, depth ('h') and TJ stress, d) energy changes and the kinetic data for the dihedral angle in semi-log scale.

as:

$$P_i = -\frac{(1-\nu^2)}{2E}\Im_i \sum_{j=0}^{n-1}\frac{\sigma_{h,ij}^2}{n}v_{ij} \quad \Rightarrow \quad \bar{P}_i = -w_o \ell_o^2 \bar{\Im}_i \sum_{j=0}^{n-1}\frac{\bar{\sigma}_{h,ij}^2}{n}\bar{v}_{ij} \qquad (5)$$

Here, $\bar{P}_i \equiv \tau_o P_i$ and $w_o \equiv (1-\nu^2)\sigma_o^2/2E$ is the nominal elastic strain energy density, and $E/(1-\nu^2)$ is the plain strain elastic modulus, $\bar{\Im}_i$ is the total scaled temporal length of the top surface of bi-crystal modulus including groove region at a given time step *i*, and with *j* standing for the collocation nodes of discrete surface. $\bar{\sigma}_{h,ij} \equiv (\sigma_{h,ij}/\sigma_o)$ and $\bar{v}_{ij}$ are the calculated normalized hoop stresses and velocities at each node. The summation is performed over the free surface contour line exposed to the surface drift diffusion. Then, the cumulative elastic strain energy relaxation (dissipation) of the body $\Delta E < 0$, which is according to Clapeyron's theorem [32, 33] compensated by one-halve of the work done on the isobaric system, may be calculated as a function of discrete normalized time $\bar{t}_i$ by a simple integration (*i.e.*, summation) procedure applied to above expression:

$$\Delta E_i \equiv \Delta \bar{E}_i = \bar{t}_i \sum_{k=0}^{i}\frac{\bar{P}_k}{i} < 0 \qquad (6)$$

The relationship in Eq. (6) is utilized to compute the total elastic strain energy relaxation, which is equal to the cumulative strain energy stored $\Delta \bar{W}_i^e$ in the body with an inverted sign $\Delta \bar{W}_i^e = -\Delta \bar{E}_i > 0$, and then the results are plotted in Figure 4d. The corresponding change in the bulk Gibbs free energy of a Hookian elastic solid is given by [33] $\Delta \bar{G}_i^b \cong \Delta \bar{F}_i^{Th} - \Delta \bar{W}_i^e \Rightarrow \Delta \bar{E}_i < 0$, assuming that the entropy density is not a sensitive function of strain. Here, $\Delta \bar{F}_i^{Th} \to 0$ is the thermal part of Helmholtz free energy, which is identically equal to zero for the isothermal changes. On the other hand, the global variations in the film surface free energy (capillary) including the shortening of the GB layer may be computed by the following equation:

$$\Delta \bar{G}_i^s = w_o \ell^* \left\{ \left(\bar{\Im}_i - \bar{L}_o \right) - 2\lambda \bar{h}_i \right\} \qquad \text{(referred to the initial dead loaded state)} \quad (7)$$

Here, $\ell^* \equiv \ell_o \Sigma^{-1}$ is the characteristic length, $\bar{h}_i$ is the

temporal normalized depth measured from the original flat surface, and $\bar{L}_o$ is the initial flat top surface length. Then the global Gibbs free energy variations during GB grooving process as referred to the initial dead loaded state may be calculated from the following formula in real time and metric space, where $\Delta G_i^s \equiv \ell_o^2 \Delta \bar{G}_i^s$ and $\Delta G_i^b \equiv \ell_o \Delta \bar{G}_i^b$:

$$\Delta G_i^T = \Delta G_i^s - \Delta W_i^e = \Delta G_i^s + \Delta E_i \overset{?}{\leq} 0 \qquad \text{(referred to the initial dead loaded state)} \quad (8)$$

The free energy changes, which are normalized with respect to common cofactor $\left[w_o \ell_o^2\right]$ are given in Figure 2f, indicate that the absolute value of the cumulative strain energy relaxation increases monotonically as the surface roughness increases. On the contrary, the change in the global Gibbs free energy strictly follows the change in the surface free energy (due to the increase in the surface area), which makes a minima in negative scale and then monotonically increases to assume positive values. This anomalous situation as may be seen from Figures 3d and 4d is more critical for the higher stress levels, where one hardly can observe any dip in the global Gibbs free energy change. The global Gibbs free energy plots clearly show that the isothermal ridge growth process taking place above the TJ-velocity inversion point (See; the cross-over in Figures 3d and 4d) is energetically unfavorable.

Therefore, it is rather a kinetically driven process, which dominates the whole ridge growth stage. This also gives us a hint that the ridge growth stage is not controlled by Ziegler's [34] 'maximum entropy production principle, designated as $Td^2\Delta S/dt^2 \leq 0 \Rightarrow\ d^2\Delta G/dt^2 \geq 0$, but by the 'minimum entropy production hypothesis, characterized by $Td^2\Delta S/dt^2 \geq 0 \Rightarrow d^2\Delta G/dt^2 \leq 0$, as formulated by Prigogine [31] for the stationary weakly non-equilibrium states in linear complex systems, which are now exposed to fixed body forces and surface tractions.

In Figures 3 and 4, we presented the effect of an increase in the stress (EDTI) on the growth kinetics of a GB groove by surface diffusion under compressive stress fields. In each case distance 'd' reaches a constant value, which is inversely proportional to the applied stress and similarly the value of the crossover depth decreases as stress increases. The amplitude of the secondary oscillations on both sides of the groove root rapidly increases with the applied stress during this kinetically driven evolution so that one may speak of extremely high surface instability above certain values.

An analysis of crossover depths 'h_c' and inversion-times collected for different levels of applied stresses may provide an analytical expression for the incubation time for ridge formation or may give an estimation of the time and depth, where grain boundary migration may start to occur if it is possible, as in the case of Genin's [6] model.

Such an analysis is presented in in Figure 5 and following equations are obtained by linear regression:

$$\bar{h}_c \cong 0.096\left|\Xi\right|^{-1/3} \quad (9)$$

$$\bar{t}_c \cong \begin{cases} 0.0062\left|\Xi\right|^{-3/2}; & \Xi \leq 1.0 \\ 0.0058\left|\Xi\right|^{-4/5}; & \Xi > 1.0 \end{cases} \quad (10)$$

Reverting back into the real time and space the above equations yield into:

$$h_c \cong \left(\frac{0.002 g_s^o \ell_o^2}{\left|tr(\underline{\underline{\lambda}}_s)\right|(1+\nu)\sigma_o} \right)^{1/3} \quad (11)$$

$$t_c \cong \begin{cases} \dfrac{0.035kT}{D_\sigma h_\sigma \Omega_\sigma} \left(\dfrac{\ell_o^{3/2} g_s^{o3/8}}{\left|tr(\underline{\underline{\lambda}}_s)\right|(1+\nu)\sigma_o} \right)^{3/2}; & \sigma_o \leq \dfrac{3g_s^o}{\left|tr(\underline{\underline{\lambda}}_s)\right|(1+\nu)\ell_o} \\ \dfrac{0.014kT}{D_\sigma h_\sigma \Omega_\sigma} \left(\dfrac{\ell_o^4 g_s^{o-1/4}}{\left|tr(\underline{\underline{\lambda}}_s)\right|(1+\nu)\sigma_o} \right)^{4/5}; & \sigma_o > \dfrac{3g_s^o}{\left|tr(\underline{\underline{\lambda}}_s)\right|(1+\nu)\ell_o} \end{cases} \quad (12)$$

Figure 5b clearly shows that the crossover time plot has a very sharp knee at $\Xi_c \equiv \left\{\ell_o u_{EDTI}/g_s\right\} = 1$. Based on

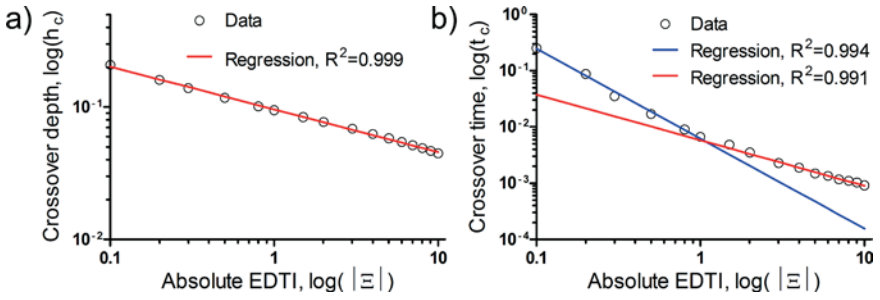

Figure 5. (Color online) Analysis of the crossover depth 'hc' and corresponding time as a function of the applied stress.

this information one can conclude that this parameter, in addition to the size of the specimen, is directly connected to the ratio of the EDTI and the surface Gibbs free energy densities. Thus it may be used as a threshold signature to separate the capillary and stress dominating regimes for the GB-ridge growth process under the uniaxial compressive stresses. This parameter also shows that the small specimen size pushes the system towards the capillary regime where the incubation time for the ridge formation stretches to longer times in logarithmic scale (i.e., apparent stagnation), just the contrary to the one should expect a priory.

CONCLUSIONS

In this study, we simulated and analyzed the surface morphological evolution kinetics associated with the GB-ridge formation and growth, in finite size bicrystal thin films under the applied uniaxial compressive stresses. In our simulations, the elastic dipole tensor interaction, between the strain field of mobile atomic species at the surface layer and the local stress field induced by the applied constant surface tractions and body forces, is considered to be the primary driving source rather than the gradient of the elastic strain energy density inhomogeneities. The most important outcomes of the extensive computer simulation studies may be outlined as follows:

1. On the contrary to the ESED, the use of gradient of the EDTI energy between the stress field and the mobile atomic species as a driving force for the surface drift-diffusion provides direct means to observe effects of compressive stresses on the evolution of bicrystal thin films for relatively small strength levels $\sigma_o \cong \{13.25(Cu) \text{ and } 2.86\ (Al)\}$ MPa .
2. The effect of an applied stress field on GB grooving in thin film bamboo lines is studied in a wide range of EDTI parameters: Ξ = [–0.1, … , –10], which correspond to [–13.25, … , –1325] MPa for copper and [–2.96, … , –296] MPa for aluminum with scaling length of ℓ_o=0.1 μm. The application of compressive stresses slows down the groove penetration but rather favors development of grain boundary ridge profiles that are in accord with the results obtained by Genin et al. [1].
3. The present non-equilibrium thermokinetics theory has shown great potential for describing the growth kinetics of experimentally observed ridges in thin films through surface diffusion. However, there is still room for improvement by considering the grain boundary flux injection to GB-TJ by the applied stress system.
4. The grain boundary area increases during the ridge growth and such a process through an immobile boundary (normal to the initial film surface) is energetically unfavorable. Thus, a more complete model should be accounted for the GB migration (grain growth), which will be our future objective via the incorporation of TJ transverse motion. Yet in this study, an incubation time for hillock growth and a crossover depth, over which GB migration becomes energetically favorable, are defined and discussed by staying within the limits of the present model. For λ=0.5, the crossover depth is found to be proportional with $\sigma^{-1/3}$. It is also found that the stress dependence of the incubation time for hillock growth distinguishes between high and low stresses, and is proportional to $\sigma^{-3/2}$ and $\sigma^{-4/5}$, respectively.
5. Since the global Gibbs free energy increases rather than the decrease monotonically, the ridge growth stage is not controlled by Ziegler's 'maximum entropy production principle' [34] but rather by the 'minimum entropy production principle' as postulated by Prigogine [31] for the stationary weakly non-equilibrium states in complex systems, which are now exposed to preset fixed body forces and surface tractions.
6. These results indicate that, the application of bi-axial compressive stresses to the ultra-fine grain poly-crystalline thin films might be a good strategy to develop network of honeycomb shape ridge structures (quasi-quantum rings), which may show strong interface confinement to achieve certain unusual electronic and optical properties due to their particular 3D topology. This type of ridge assembly having almost honeycomb style pattern after the elevated temperature annealing treatment may offer a chance to study the magnetic behavior of susceptibility and the Aharonov-Bohm effect [35].

ACKNOWLEDGEMENTS

The authors wish to thank Professors Şakir Bor and Güngör Gündüz of Middle Technical University (METU) for their constant interest and valuable advice in this project. This work was partially supported by the Turkish Scientific and Technological Research Council, TUBITAK through a research Grant No. 107M011.

REFERENCES

1. Genin FY, Mullins WW, Wynblatt P. The effect of stress on grain boundary grooving. Acta Metall Mater 41 (1993) 3541-3547. doi: 10.1016/0956-7151(93)90234-J
2. Mullins WW. Theory of Thermal Grooving. J Appl Phys 28 (1957) 333. doi: 10.1063/1.1722742
3. Philofsky E, Ravi K, Hall E, Black J. Surface Reconstruction of Aluminum Metallization –– a New Potential Wearout Mechanism. 9th Reliab. Phys. Symp. IEEE, pp 120-128, 1971.

4. Chang CY, Vook RW, Lee YC, Hoshi I. Isothermal annealing of hillocks in Al–Cu films. Thin Solid Films 181 (1989) 57–63. doi: 10.1016/0040–6090(89)90472–0
5. Ericson F, Kristensen N, Schweitz J–A, Smith U. A transmission electron microscopy study of hillocks in thin aluminum films. J Vac Sci Technol B Microelectron Nanom Struct 9 (1991) 58. doi: 10.1116/1.585790
6. Genin FY. Effect of stress on grain boundary motion in thin films. J Appl Phys 77 (1995) 5130. doi: 10.1063/1.359324
7. 7. Genin FY. The initial stages of the formation of holes and hillocks in thin films under equal biaxial stress. Acta Metall Mater 43 (1995) 4289–4300. doi: 10.1016/0956–7151(95)00132–F
8. Genin FY, Siekhaus W. Experimental study to validate a model of hillock's formation in aluminum thin films. J. Appl. Phys. 79 (1996) 3560–3566.
9. Kim D, Nix WD, Vinci RP, Deal MD, Plummer JD. Study of the effect of grain boundary migration on hillock formation in Al thin films. J Appl Phys 90 (2001) 781. doi: 10.1063/1.1381045
10. Chaudhari P. Hillock growth in thin films. J Appl Phys 45 (1974) 4339. doi: 10.1063/1.1663054
11. Presland AEB, Price GL, Trimm DL. Hillock formation by surface diffusion on thin silver films. Surf Sci 29 (1972) 424–434. doi: 10.1016/0039–6028(72)90229–4
12. Hull D, Rimmer DE. The growth of grain–boundary voids under stress. Philos Mag 4 (1959) 673–687. doi: 10.1080/14786435908243264
13. Gao H, Zhang L, Nix WD, Thompson CV, Arzt E. Crack–like grain–boundary diffusion wedges in thin metal films. Acta Mater 47 (1999) 2865–2878. doi: 10.1016/S1359–6454(99)00178–0
14. Zhang L, Gao H. Coupled grain boundary and surface diffusion in a polycrystalline thin film constrained by substrate. Zeitschrift für Met 93 (2002) 417.
15. Barvosa–Carter W, Aziz MJ, Gray LJ, Kaplan T. Kinetically driven growth instability in stressed solids. Phys Rev Lett 81 (1998) 1445–1448. doi: 10.1103/PhysRevLett.81.1445
16. Lahiri SK. Stress Relief and Hillock Formation in Thin Lead Films. J Appl Phys 41 (1970) 3172. doi: 10.1063/1.1659383
17. Ogurtani TO. Unified theory of linear instability of anisotropic surfaces and interfaces under capillary, electrostatic, and elastostatic forces: The regrowth of epitaxial amorphous silicon. Phys Rev B 74 (2006) 1–25. doi: 10.1103/PhysRevB.74.155422
18. Kirchheim R. Stress and electromigration in Al–lines of integrated circuits. Acta Metall Mater 40 (1992) 309–323. doi: 10.1016/0956–7151(92)90305–X
19. Basaran C, Lin M, Ye H. A thermodynamic model for electrical current induced damage. Int J Solids Struct 40 (2003) 7315–7327. doi: 10.1016/j.ijsolstr.2003.08.018
20. Sukharev V, Nix WD, Zschech E. A model for electromigration–induced degradation mechanisms in dual–inlaid copper interconnects: Effect of microstructure. J Appl Phys 102 (2007) 053505. doi: 10.1063/1.2775538
21. Akyildiz O, Oren EE, Ogurtani TO. Grain boundary grooving in bi–crystal thin films induced by surface drift–diffusion driven by capillary forces and applied uniaxial tensile stresses. Philos Mag 92 (2012) 804–829. doi: 10.1080/14786435.2011.634850
22. Ogurtani TO. Mesoscopic nonequilibrium thermodynamics of solid surfaces and interfaces with triple junction singularities under the capillary and electromigration forces in anisotropic three–dimensional space. J Chem Phys 124 (2006) 144706. doi: 10.1063/1.2185625
23. Ogurtani TO, Oren EE. Irreversible thermodynamics of triple junctions during the intergranular void motion under the electromigration forces. Int J Solids Struct 42 (2005) 3918–3952. doi: 10.1016/j.ijsolstr.2004.11.013
24. Ogurtani TO, Akyildiz O. Morphological evolution of voids by surface drift diffusion driven by capillary, electromigration, and thermal–stress gradients induced by steady–state heat flow in passivated metallic thin films and flip chip solder joints. I. Theory. J Appl Phys 104 (2008) 023521. doi: 10.1063/1.2958088
25. Ogurtani TO, Akyildiz O. Morphological evolution of voids by surface drift diffusion driven by the capillary, electromigration, and thermal–stress gradient induced by the steady state heat flow in passivated metallic thin films and flip–chip solder joints. II. Applications. J Appl Phys 104 (2008) 023522. doi: 10.1063/1.2958303
26. Yeremin EN. The Foundations of Chemical Kinetics. MIR Publishers, Moscow, Russia , 1979.
27. Beer G, Watson JO. Introduction To Finite And Boundary Element Methods For Engineers. John Wiley & Sons, New York, USA, 1992.
28. Gear CW. Numerical initial value problems in ordinary differential equations. Prentice–Hall, Englewood Cliffs, N. J., 1971.
29. Pan J, Cocks ACF. A numerical technique for the analysis of coupled surface and grain–boundary diffusion. Acta Metall Mater 43 (1995) 1395–1406. doi: 10.1016/0956–7151(94)00365–O
30. Friesen C. Reversible stress changes at all stages of Volmer–Weber film growth. J Appl Phys 95 (2004) 1011. doi: 10.1063/1.1637728
31. Prigogine I. Introduction to Thermodynamics of Irreversible Processes. Interscience Publishers, New York, USA, 1961.
32. Ogurtani TO, Celik A, Oren EE. Morphological evolution in a strained–heteroepitaxial solid droplet on a rigid substrate: Dynamical simulations. J Appl Phys 108 (2010) 063527. doi: 10.1063/1.3483937
33. Sokolnikoff I. Mathematical Theory of Elasticity. McGraw–Hill Book Co., New York, 1956.
34. Martyushev LM, Seleznev VD. Maximum entropy production principle in physics, chemistry and biology. Phys Rep 426 (2006) 1–45. doi: 10.1016/j.physrep.2005.12.001
35. Aharonov Y, Bohm D. Significance of electromagnetic potentials in the quantum theory. Phys Rev 115 (1959) 485–491. doi: 10.1103/PhysRev.115.485
36. Kröner E. Kontinuums theorie der Versetzungen und Eigenspannungen. Springer, Berlin, 1958.
37. Hong QZ, Zhu JG, Mayer JW, Xia W, Lau SS. Solid phase epitaxy of stressed and stress–relaxed Ge–Si alloys. J Appl Phys 71 (1992) 1768. doi: 10.1063/1.351212
38. Smithells CJ. Metals Reference Book Vol. 3. Butterworths, London, 1967.

Appendix

The elastic dipole tensor concept was first introduced by Late Professor Kröner [36] for the elastic strain field interaction between point defects and the applied stress fields in bulk phases, which may be formulated as $u^{*}_{EDTI} = -\Omega_a \underline{\underline{\lambda}} : \underline{\sigma}$ The tetrahedral elastic dipole tensor associated with these so-called paraelastic defects may be described by: $\underline{\underline{\lambda}}^{*}_{\hat{q}} = \lambda_1 \left[\underline{\underline{I}} + \eta \delta_{(n)q} \delta_{(n)m} \right]$ where $q = 3$ denotes direction of the symmetry axis and $\eta = (\lambda_3 - \lambda_1)/\lambda_1$ is closely related to the shape factor. λ_3, $\lambda_1 = \lambda_2$ are the principal values of the tetragonal elastic dipole tensor, along the symmetry axis denoted by $\hat{q}$ and in the interface tangent plane (transverse components), respectively. $\delta_{(n)q}$ is Kronecker deltafunction, $\hat{q}$ denotes the direction of the tetragonal axis, which is parallel to the interface normal $\hat{n}$ for the present case, and $(.)$ indicates that the Einsteinsummation rule for the repeated indices is not valid. Then one can easily show that the EDTI energy may be given by the following expression $u^{*}_{EDI} = -\Omega \lambda \underline{\underline{\lambda}} : \underline{\sigma}$ $= -\Omega \lambda_1 (Tr\underline{\sigma} + \eta \sigma_{qq})$ for the general stress systems, where $\sigma_{qq} \equiv \hat{q}.\underline{\sigma}.\hat{q}$, and it is equal to zero for the traction free surfaces. As a special case; the uniaxial stress system acting in the surface tangent plane in the direction of $\hat{t}$, one can obtain the following expression for EDTI energy: $u^{*}_{EDI} = -\Omega \lambda_1 \sigma_{\tilde{t}\tilde{t}}$, where $Tr\sigma \Rightarrow \sigma_{\tilde{t}\tilde{t}}$ is called hoop stress in engineering applications. The general formula given previously, clearly shows that one cannot consider the application of the pure hydrostatic stress (whether it is hydrostatic pressure or triaxial tension) $\underline{\sigma} = -p\underline{I}$ on the composite system (solid/fluid and solid/amorphous), without violating the mostly used traction free boundary conditions. In the case of biaxial stress system acting in the surface tangent plane one can also obtain the following expression for EDTI energy: $u^{*}_{EDI} = -2\Omega \lambda_1 \sigma_{\tilde{t}\tilde{t}}$. This shows that the biaxial in-plane stress has twice the effect of uniaxial stress as confirmed experimentally by Hong et al. [37].